



CHORUS

This is the accepted manuscript made available via CHORUS. The article has been published as:

Optical investigation of the strong spin-orbit-coupled magnetic semimetal YbMnBi_2

Dipanjan Chaudhuri, Bing Cheng, Alexander Yaresko, Quinn D. Gibson, R. J. Cava, and N. P. Armitage

Phys. Rev. B **96**, 075151 — Published 24 August 2017

DOI: [10.1103/PhysRevB.96.075151](https://doi.org/10.1103/PhysRevB.96.075151)

An optical investigation of the strong spin-orbital coupled magnetic semimetal YbMnBi_2

Dipanjan Chaudhuri,¹ Bing Cheng,¹ Alexander Yaresko,² Quinn D. Gibson,³ R. J. Cava,³ and N. P. Armitage¹

¹*Department of Physics and Astronomy, The Johns Hopkins University, Baltimore, MD 21218, USA*

²*Max-Planck-Institute for Solid State Research, Heisenbergstrasse 1, 70569 Stuttgart, Germany*

³*Department of Chemistry, Princeton University, Princeton, NJ 08544, USA*

Strong spin-orbit coupling (SOC) can result in ground states with non-trivial topological properties. The situation is even richer in magnetic systems where the magnetic ordering can potentially have strong influence over the electronic band structure. The class of AMnBi_2 ($A = \text{Sr}, \text{Ca}$) compounds are important in this context as they are known to host massive Dirac fermions with strongly anisotropic dispersion, which is believed to be due to the interplay between strong SOC and magnetic degrees of freedom. We report the optical conductivity of YbMnBi_2 , a newly discovered member of this family and a proposed Weyl semi-metal (WSM) candidate with broken time reversal symmetry. Together with density functional theory (DFT) band structure calculations, we show that the complex conductivity can be interpreted as the sum of an intra-band Drude response and inter-band transitions. We argue that the canting of the magnetic moments that has been proposed to be essential for the realization of the WSM in an otherwise antiferromagnetically ordered system is not necessary to explain the optical conductivity. We believe our data is explained qualitatively by the uncanted magnetic structure with a small offset of the chemical potential from strict stoichiometry. We find no definitive evidence of a bulk Weyl nodes. Instead we see signatures of a gapped Dirac dispersion, common in other members of AMnBi_2 family or compounds with similar 2D network of Bi atoms. We speculate that the evidence for a WSM seen in ARPES arises through a surface magnetic phase. Such an assumption reconciles all known experimental data.

I. INTRODUCTION

Correlated electron systems with strong SOC have been the subject of intensive research in recent years. The interplay of electronic correlations and SOC can result in emergent topological phases and has opened up a completely new direction in condensed matter physics. This interplay can be very different depending on the specifics of the electronic correlation. In weakly to moderately interacting electron systems, SOC can lead to non-trivial band topology as observed in conventional topological insulators¹, Dirac and Weyl semi-metals²⁻⁴, axion insulators⁵ and topological superconductors⁶. More recently, the effects of SOC on strongly correlated systems are being explored with the realization of new material systems with heavy 4d/5d transition metal compounds⁷. The iridates deserve special mention in this category and have been instrumental in exploring much of this uncharted territory^{8,9}.

In addition to the emergence of topologically non-trivial ground states, the interplay between SOC and magnetic degrees of freedom themselves is also quite interesting. The family of AMnBi_2 ($A = \text{Sr}, \text{Ca}$) compounds are particularly important in this context. Being structurally similar to iron based superconductors, they are referred to as manganese pnictides, which contain layers of Mn-Bi edge sharing tetrahedra and a Bi square net separated by a layer of A atoms¹⁰. These compounds were expected from first principles DFT band calculations to host highly anisotropic Dirac dispersions with a finite gap at the Dirac point due to SOC¹¹. Such predictions were confirmed experimentally through magnetization, magneto-transport measurements^{12,13} and

later using angle resolved photoemission spectroscopy (ARPES)¹⁴. What makes these compounds particularly interesting is the antiferromagnetic (AFM) ordering of the spin magnetic moment on the Mn^{2+} atoms which has a $3d^5$ electronic configuration. The magnitude of the ordered moment is around $4\mu_B$ with an ordering temperature $\sim 300\text{K}$ as observed in several experiments^{10,11}. Strong in-plane super exchange is responsible for the Néel-type AFM ordering observed in the ab plane with a rather weak inter-layer magnetic coupling whose nature is dependent on the A atom¹⁰.

More recently, new members have been added to this family by substituting the rare earth elements with lanthanides such as Europium and Ytterbium. Whereas EuMnBi_2 appears to be very similar to its rare earth sister compounds¹⁵, YbMnBi_2 appears to have richer behavior and has been proposed as a prospective candidate for type II Weyl semi-metal (WSM)¹⁶. Unlike most WSMs discovered so far that are non-centrosymmetric systems (TaAs , NbAs , NbP , TaP , SrSi_2 , etc) with broken inversion symmetry, YbMnBi_2 has been proposed to be a potential WSM with broken time reversal symmetry (TRS). A magnetic WSM has continued to be elusive to date, with the possible exception of potential WSM phases in pyrochlore iridates¹⁷ and magnetic heuslers under magnetic field¹⁸. In contrast to the other members of the AMnBi_2 family, ARPES has shown a Fermi surface that appears to be continuous with the hole-like lenses touching the electron-like pockets at what has been interpreted to be the Weyl nodes. It should be noted, that the band structure calculations predict that a TRS breaking WSM state can only be realized in this compound if a canting of the magnetic moment ($\sim 10^\circ$) from the c

axis, resulting in an effective in-plane ferromagnetic component along (110) direction, is assumed in addition to the established AFM ordering. Although such a band structure is in reasonable agreement with the ARPES results, the ad-hoc assumption of canted antiferromagnetism has not been supported by neutron scattering experiments^{19,20}. Moreover, the magnetic space group found via neutron scattering that describes the AFM ordering in YbMnBi₂ has a symmetry breaking that does not allow canting of Mn magnetic moments away from the *c* axis. From general considerations, the only way canting can occur is via an AFM transition that is not second order, or a lattice symmetry that is not tetragonal. Transport measurements reported in²⁰ further supports a quasi two dimensional Dirac dispersion in this compound.

A number of interesting proposals have been made for the optical properties of WSMs²¹. An ideal 3D Weyl state comprises at least a pair of non-degenerate band crossings in momentum space with the Fermi level at the nodal point. In 3D Dirac or Weyl systems, the joint density of states increases with frequency and is proportional to ω^2 whereas the dipole optical matrix element goes as ω^{-1} as a result of which at low frequencies, the real optical conductivity is linear in ω . In real systems however it is hard to achieve such fine tuning in the Fermi energy (E_F) and hence a cut-off is set by the Fermi level such that the real part of the conductivity is expected to be

$$\sigma_1(\omega) = \frac{NG_0\omega}{24v_F}\Theta(\omega - 2E_F). \quad (1)$$

where N is the number of massless fermion species in the Brillouin zone, $G_0 = 2e^2/h$ is the quantum conductance and v_F is the Fermi velocity. Experimental evidence of such linear optical conductivity with zero intercepts has been reported in Eu₂Ir₂O₇¹⁷ and TaAs²² among others⁴. A more detailed theoretical analysis of the inter-band optical response of TRS breaking WSMs²³ however predicts that the single linear optical conductivity should be broken into two regions of quasi-linear conductivity with different slopes by a peculiar kink. The kink is a manifestation of the van Hove singularity, appearing at a frequency that corresponds to the energy difference between the bands crossing to form the Weyl nodes at the extrema between the two nodes. Such a feature has been experimentally observed in the inversion symmetry broken WSM TaAs²².

In this paper, we report the complex optical conductivity of YbMnBi₂²⁴ obtained from Kramers-Kronig (KK) constrained variational dielectric function (VDF) fitting of the reflectivity. A comparison of the experimental optical spectra with that calculated from the DFT band structure shows that the low energy features in the spectrum can be attributed to specific inter-band transitions and are not a signature of the van Hove singularity as proposed elsewhere²⁵. The optical spectra has also been compared to the calculated band structures with both canted and uncanted AFM ordering which opens the pos-

sibility of reconciling the ARPES experiments with the neutron scattering and transport results. We believe our optical data is explained qualitatively by the uncanted magnetic structure with a small offset of the chemical potential from strict stoichiometry.

II. EXPERIMENTAL AND COMPUTATIONAL DETAILS

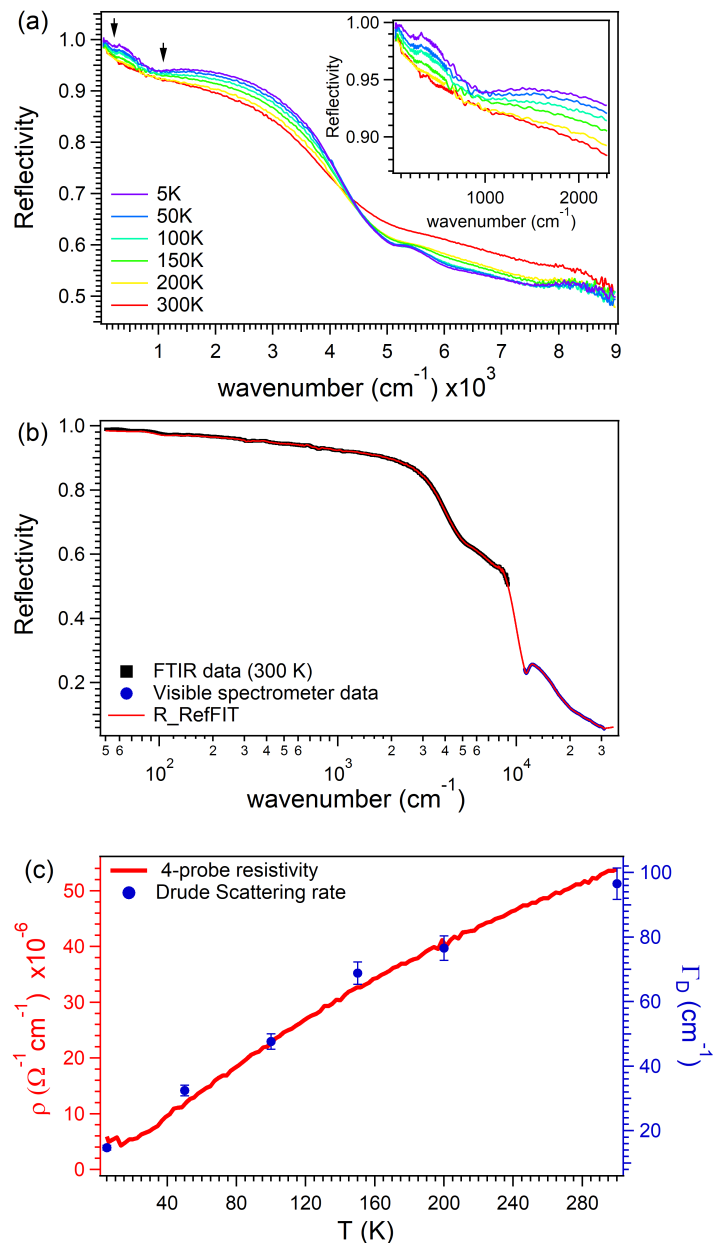


Figure 1. (a) Reflectivity of YbMnBi₂ measured using FTIR spectroscopy for different temperatures. (inset) Expanded plot showing the low-frequency region. (b) Raw reflectivity data at 300 K along with reflectivity curve as obtained from VDF fitting. (c) Resistivity of the sample measured using a 4-probe technique along with the Drude scattering rates.

Optical properties were measured on a cleaved (001) surface ($\sim 3 \text{ mm} \times 3 \text{ mm}$) of a high quality YbMnBi_2 crystal using Fourier transform infrared (FTIR) spectroscopy. For details of the sample preparation please refer to Ref.¹⁶. The as-grown (001) surface of another slightly smaller crystal was also measured and had identical results. Fourier transform spectroscopy is known to offer excellent signal to noise and frequency resolution. Reflectivity of YbMnBi_2 single crystals were measured using a commercial FTIR spectrometer (Bruker, Vertex 80V, Source: Globar/Hg Arc Lamp, Detectors: DLaTGS/MCT/Bolometer) across far and mid infrared spectral ranges spanning from 50 cm^{-1} to 8500 cm^{-1} (i.e. 1.5-2500 THz) for several temperatures between 5 K and 300 K. The reflection spectra at each temperature were referenced to that of elemental gold, deposited on the sample in situ by thermal evaporation. To extend the measurement across a broader spectral range, the infrared spectra was supplemented by visible reflection spectrum between 11150 cm^{-1} and 29000 cm^{-1} measured at room temperature using commercial spectrophotometry (Hitachi, U-3010) and referenced to an aluminum mirror. Additionally, the DC resistivity of the sample has been measured using conventional 4-probe measurements down to 2K.

Figure 1(a) shows the measured reflectivity in the infrared regime. The reflectivity tends to 1 at low frequencies and drops with a broad plasma edge-like feature above 4000 cm^{-1} indicating metallic behavior. Besides the usual Drude response, two distinct features are observed in the reflectivity spectra that becomes particularly prominent at low temperatures. The lowest one is close to 200 cm^{-1} where there is an abnormal increase in reflectivity and the second feature is a rather broad bump around 950 cm^{-1} .

Band structure calculations were performed using the linear muffin-tin orbital method²⁶ as implemented in the relativistic PY LMTO computer code. Some details of the implementation can be found in Ref. 27. Calculations were done assuming collinear AFM ordering of Mn moments which were aligned along the c axis. Completely filled $\text{Yb}^{2+} 4f^{14}$ states were treated as semi-core states. SOC was added to the LMTO Hamiltonian in the variational step. All theoretical results presented below were obtained within the local spin-density approximation (LSDA) with the Perdew-Wang parameterization²⁸ for the exchange-correlation potential. Test calculations were also done using the PBE GGA potential.²⁹ They showed that the use of GGA slightly increases exchange splitting of Mn d states but has only minor effect on Bi p derived bands. Brillouin zone (BZ) integrations during the self-consistency loop were done on a $32 \times 32 \times 16$ mesh using the improved tetrahedron method.³⁰

Matrix elements for interband optical transitions were calculated in the dipole approximation. Then, the real part of the optical conductivity was calculated using the tetrahedron method and the imaginary part was obtained using the Kramers-Kronig relations.

We found that a very dense k mesh should be used in order to achieve convergence of the conductivity below 0.3 eV. For instance, the in-plane conductivity spectrum calculated on the $32 \times 32 \times 16$ mesh shows a broad peak centered at 0.18 eV. The peak shifts to $\sim 0.10 \text{ eV}$ ($\sim 1000 \text{ cm}^{-1}$), becomes narrower, and its height doubles when a denser $80 \times 80 \times 48$ mesh with almost 40000 symmetry inequivalent k points in BZ is used. The use of even denser $128 \times 128 \times 48$ ($\sim 10^6$ k points) mesh still leads to a small ($< 0.01 \text{ eV}$) shift of the peak position and 10% increase of its height. However, since calculations on such a dense mesh becomes extremely time consuming we present in the next section conductivity spectra calculated on the $80 \times 80 \times 48$ mesh. It is worth noting, that above 0.5 eV convergence of the calculated conductivity spectrum is achieved already on the $32 \times 32 \times 16$ mesh.

III. ANALYSIS AND RESULTS

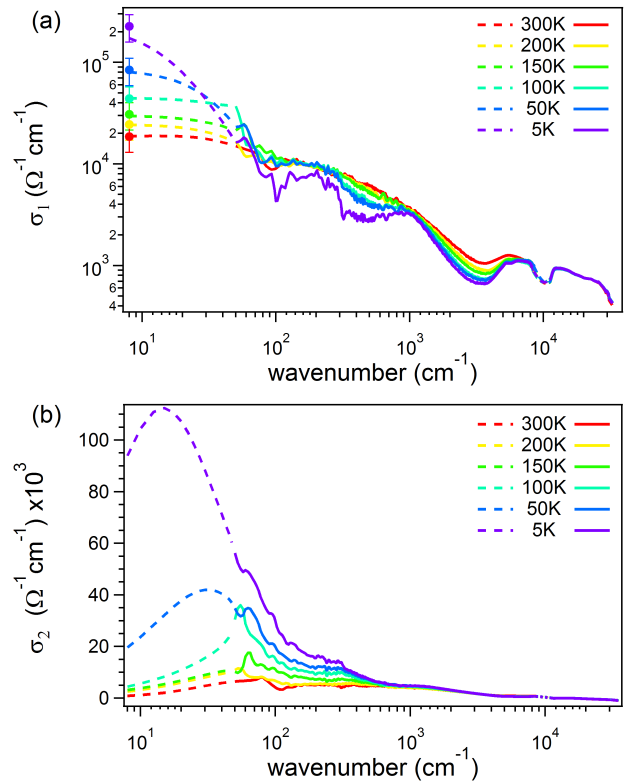


Figure 2. (a) Real and (b) imaginary part of conductivity. Solid and dashed lines represent the measured and extrapolated frequency regimes respectively. The markers at 8 cm^{-1} in (a) represents the dc conductivity calculated from 1(c)

The complex optical conductivity of the sample has been calculated from the reflectivity spectrum using KK constrained VDF fitting³¹. This technique is an alternative to using conventional KK transformations to calculate the complex conductivity from a single measurement and is particularly useful in dealing with multiple

reflection/transmission data from different disjoint frequency ranges. The method, implemented using the software RefFIT, involves an initial fitting of the reflectivity spectra to a standard Drude-Lorentz oscillator model with a few oscillators and then performing a KK constrained variational fitting with many oscillators of the difference spectra. For YbMnBi_2 , the reflectivity spectra for each temperature has been fitted with one Drude and six Lorentz oscillators which has then been subjected to the VDF fitting analysis. Figure 1(b) shows the actual infrared and visible reflectivity data at 300K along with the output of the VDF fitting. In addition to reflectivity, the dc conductivity at each temperature as obtained from 4-probe resistivity measurements (see figure 1(c)) have also been used to constrain the VDF fitting subroutine. The real and imaginary parts of the complex conductivity thus obtained are shown in figure 2(a) and 2(b) respectively.

We model the low frequency response ($<150 \text{ cm}^{-1}$) for all temperatures by a single Drude oscillator. Figure 1(c) shows the Drude scattering rate, Γ_D , as a function of temperature. Note that the temperature dependence of Γ_D scales as resistivity within experimental error. At low temperatures, the resistivity of YbMnBi_2 has a strong temperature dependence showing the dominant role of inelastic scattering from either electron-electron or electron-phonon interactions. The similarity in temperature dependence of resistivity and Γ_D thus points to the coherent nature of the quasiparticles within the Drude subsystem. The Drude plasma frequency at 5K as obtained from the fitting is 1.74 eV. Drude fitting of the low frequency response can be insufficient for a multi-band system where the different sets of carriers have different optical parameters, but by definition the plasma frequency is a measure of the spectral weight in the low frequency intraband part of the spectrum.

The two most prominent features in the real part of the optical conductivity are the low energy peaks around 200 cm^{-1} and 950 cm^{-1} . Such peaks in conductivity are ordinarily attributed to inter-band electronic transitions. To investigate this further, the Drude contribution (which mostly captures the intra-band optical conductivity) was subtracted. In general, strong electronic correlation can give low frequency intra-band contributions that would not generally be captured through a Drude term only. One possible way to isolate such effects is through the extended Drude model³² analysis which can account for inelastic scattering due to electron-electron or electron-phonon interactions that can be frequency dependent even at low frequencies. However, the extended Drude model is only reliable much below the energy scales of inter-band transitions and thus it is not particularly useful in this context where the lowest possible inter-band transition could be as low as 200 cm^{-1} . We will therefore ignore such effects for now and assume that all the remaining high frequency optical conductivity is primarily from inter-band transitions and compare it to the inter-band optical conductivity calculated from band

structure.

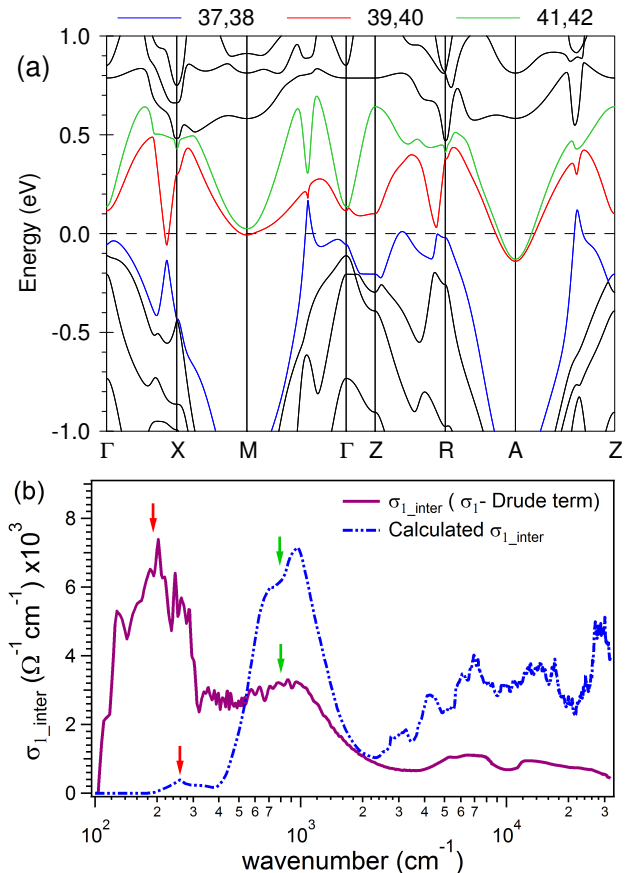


Figure 3. (a) Band structure calculated along symmetry lines in tetragonal BZ. Doubly degenerate bands near the Fermi level, discussed in the text, are plotted with blue (37,38), red (39,40), and green (41,42) lines. and (b) comparison of the calculated optical conductivity with experiment

Calculated inter-band optical conductivity (see figure 3(b)) is in rough agreement with the experimental observations at low frequencies and successfully reproduces a peak at 950 cm^{-1} (green arrows) although the predicted amplitude is much larger. However, as one can see, the calculated conductivity is significantly higher than the experimental one almost all throughout the frequency range. The origin and significance of this peak will be discussed further below.

The more striking feature is perhaps the almost complete absence of a large peak close to 200 cm^{-1} (red arrows) in the calculated optical conductivity spectra which might be indicative of some deeper inconsistencies. As the band structure in figure 3(a) does not include the canting of the Mn^{2+} moments that is believed to be necessary for the magnetic WSM phase, a next obvious step is to include that in the DFT calculations.

Figure 4(a) and 4(b) shows the band structure along (001) for a canting of 5° and 10° from the c-axis respectively. Two sets of Weyl points develop in the band structure for the canted system. The first set consists of two pair of Weyl nodes at momentum coordinates

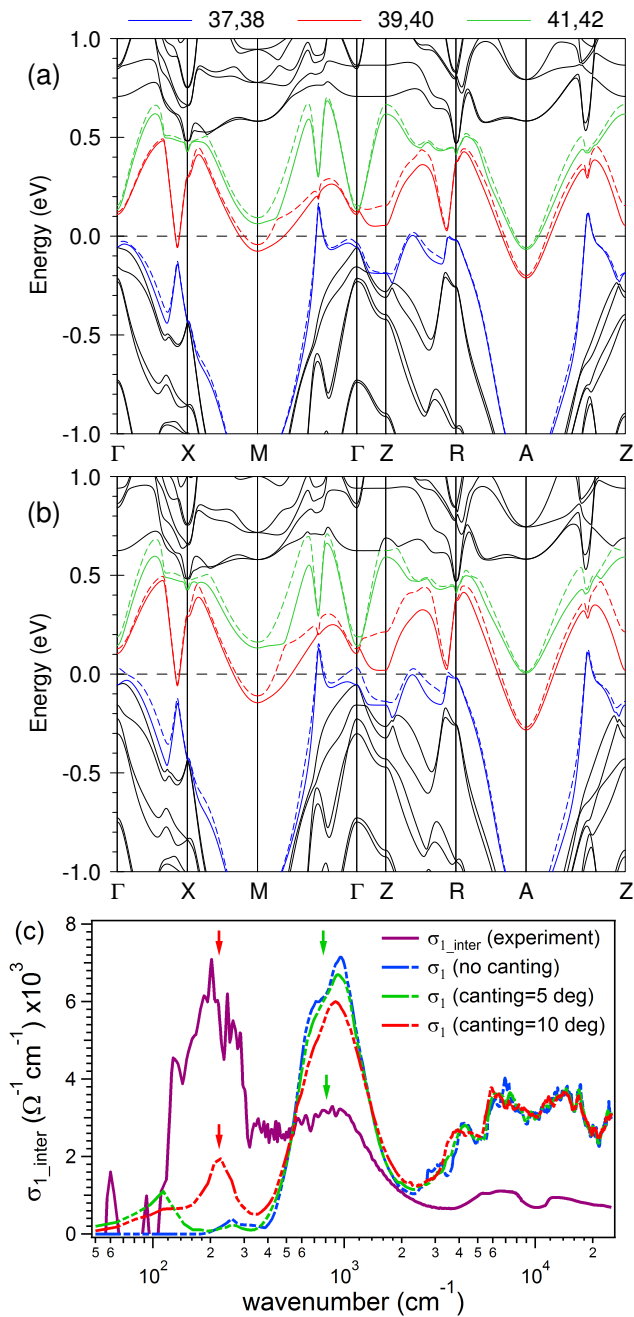


Figure 4. Band structure calculated along symmetry lines for a canting of (a) 5° and (b) 10° from the c -axis. The solid and dashed lines of the same colors represent the bands that were degenerate without canting. (c) Comparison of the calculated optical conductivity for different canting with experiment

(0.193,0.193,0.12), (0.193,0.193,-0.09) and symmetry related points. In figure 4(a) and 4(b), along the k -space cut along the M - Γ line, the Weyl point can be seen to be developing near 200 meV. The other four Weyl nodes are at (0.394, 0.045, 0.131) and symmetry related points. Details of these Weyl node structures have been discussed in reference¹⁶. Note that for all points, there are certain non-idealities (both in distortions of the bands and their position from E_F) when compared to the simplest

Weyl band structure proposed in²³ which would make the observation of Weyl physics in the optical response challenging.

The inter-band conductivity for these three levels of canting, as well as the experimental data is plotted in figure 4(c). Note that a peak slightly above 200 cm^{-1} gradually develops as one includes the effect of canting in the band structure. Nevertheless, one must be cautious in claiming this to be evidence for the WSM phase as there are noticeable alterations in the band structure unrelated to WSM physics that might bring about the observed changes in optical conductivity. The principal modification to the band structure from canting is the lifting of two fold degeneracy of the bands close to the Fermi level. This is the feature that gives rise to the Weyl nodes in the calculated band structure. However, this also opens up the possibility of having transitions between these previously degenerate bands as not all of them are above or below the Fermi level. The signatures of such inter-band transitions are not expected to be directly related to the existence of the Weyl nodes as one can see that they are generally far from the Fermi level.

If the important changes to the optical conductivity are indeed from the bands being rearranged around the Fermi level, somewhat similar changes may be observed by a shift of the chemical potential. Moreover, doping is rather common in semimetallic systems and thus exploring this possibility is important. This was investigated by shifting the chemical potential above the calculated charge neutral Fermi level (see figure 5(a)). An enhancement in the spectral weight under the calculated peak at 200 cm^{-1} is seen upon shifting chemical potential by 20 meV above the charge neutral Fermi level (see figure 5(b)). Thus it is possible that that the observed peak at 200 cm^{-1} is simply indicative of a low energy inter-band transitions and not a signature of Weyl nodes as postulated elsewhere²⁵.

To investigate the origin of these two peaks more closely, we decomposed the calculated conductivity into individual inter-band contributions. Figure 6(a) shows the result of that decomposition. These calculations provide more definitive proof to support that the peak in conductivity at 200 cm^{-1} is indeed an inter-band transition from the set of degenerate bands that is mostly above the Fermi level (bands 39, 40) to the immediate higher one (bands 41, 42). This is why when the Fermi level is shifted to higher energies, the occupation in the lower degenerate set of bands (39, 40) and consequently the transition probability increases. Hence we observe the enhancement of the amplitude of the peak in conductivity upon shifting the Fermi level and is a probable cause of the experimentally observed peak.

It is interesting to note that in the context of the conductivity calculated from the band structure with canted AFM order, the origin of the peak at 200 cm^{-1} is somewhat different than in the context of the uncanted structure, despite appearing at a similar energy scale. A decomposition into different inter-band contribution indi-

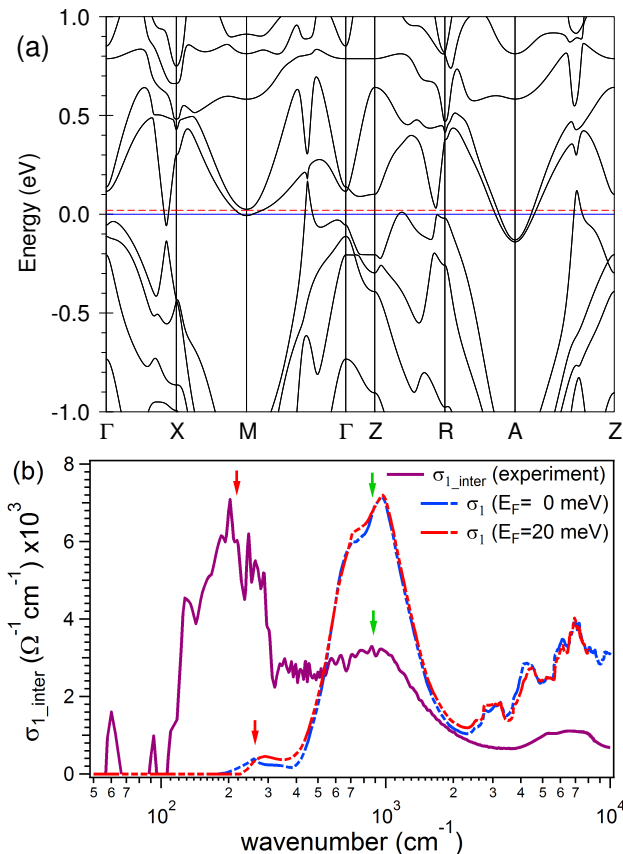


Figure 5. Band structure along (001) with Fermi level at 0 meV (blue solid line) and 20 meV above (red dashed line). (b) Calculated optical conductivity for the corresponding Fermi levels.

cates that in this structure the peak is primarily from transitions between the previously degenerate bands, i.e., bands 37→38 and 39→40 (Band labels given in Fig. 3). Although there is not much evidence from our experiment to choose one over the other, we do not favor this as the correct interpretation of our data as a canted order is not supported by neutron scattering experiments or theoretical considerations. However, this calculation further elucidates the fact that this peak is not a signature of Weyl node, even in a band structure that incorporates the effects of canted AFM order.

A possible explanation for the discrepancy in amplitude of the 200 cm^{-1} peak would be electronic correlation effects which can potentially add to the intra-band conductivity but would not be captured through simple subtraction of the Drude contribution. As an alternative to this peak being an inter-band excitation, it may arise from the coupling of conduction electrons to magnetism. Neutron scattering experiments on YbMnBi_2 ¹⁹ show prominent spin wave excitations in the energy range $\sim 120 - 340 \text{ cm}^{-1}$ which matches the energy scale of the low energy peak observed in conductivity. The extent of this coupling is hard to estimate solely from optical conductivity measurements. One can expect such correlations to redistribute the Drude spectral weight giving

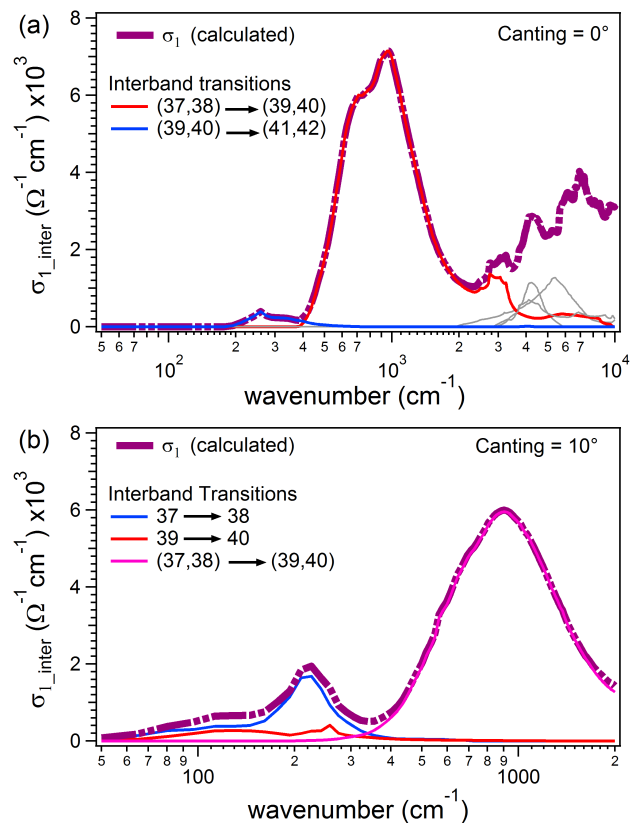


Figure 6. (a) Decomposition of the the total inter-band optical conductivity into individual band transitions. Transitions from bands (39, 40) to (41, 42) result in the peak at 200 cm^{-1} whereas transitions from bands (37, 38) to (39, 40) is the origin of the peak at 950 cm^{-1} . (b) Similar decomposition assuming a 10° canted AFM order in the band structure.

an effective mass of the quasiparticles, m^* , different from the band mass, m_b . Such mass renormalizations can be extracted using extended Drude model analysis but as argued before, it would be unreliable in the present context because of the low lying inter-band transitions. However we can roughly characterize the renormalization effect by spectral weight analysis. We make use of the conductivity sum rule

$$\frac{Z_0}{\pi^2} \int_0^{\omega_c} \sigma_1(\omega) d\omega = \omega_p^2 = \frac{4\pi n e^2}{m_b} \quad (2)$$

where Z_0 is vacuum impedance, n is the carrier density and ω_c is chosen appropriately to include the bandwidth of interest. If we interpret both the Drude term and peak at 200 cm^{-1} both as inter-band contributions, then the ratio of the total spectral weight to the Drude piece gives a measure of the renormalized mass. A naive estimate of this electron-magnon coupling constant from this exercise, $\gamma = m^*/m_b - 1 = 0.4$. This is however a rather crude estimate as we know that there is a finite contribution to the conductivity at these frequencies from inter-band transitions and hence these numbers are only a rough guide. It would be interesting to estimate coupling constants from the neutron scattering data.

The peak at 950 cm^{-1} is clearly from the inter-band transition between the bands of interest that would host the Weyl nodes in the canted structure i.e., right above (39,40) and below (37,38). However, because of the other low energy transition, it is nearly impossible to isolate any signature of the Weyl nodes if they exist in the optical conductivity spectrum. The peak derives from the quasi-2D Bi p -states (see³³) and is indicative of the linear dispersion. A sharp peak in conductivity is ordinarily expected to appear if a pair of occupied initial and empty final bands have nearly parallel dispersion in a large volume in k -space. Such an energy dispersion may occur if the Fermi level is inside a gap, which opens due to avoided crossing of two bands, and the size of the gap is constant in a large part of Brillouin zone. Hence it is reasonable to conclude that this peak is a signature of a Dirac dispersion with a small mass gap. This gap between the “lens” shaped Fermi surfaces from the (37,38) bands and the “boomerang” shaped Fermi surfaces from the (39,40) bands (see figure 7(a) (inset)) extends along k_z over the whole Brillouin zone as the derived Bi p bands are quasi-2D. This is further supported by partial conductivity calculations where we have integrated over cylindrical regions in k -space centered around points shown in the inset in Fig. 7(a). The radius of each cylinder was chosen to be $\approx 0.1 \times \frac{2\pi}{a}$ and the results clearly indicate that the major contribution to this peak is from the D-point which is between the “lens” and the “boomerang” shaped Fermi surfaces where the Fermi level lies in the gap. Calculations also indicate that the magnitude of this gap does not depend on k_z as expected. The contribution from B and X-points are also quite significant but as these points are in close proximity to the D-point, it is not surprising because the cylindrical volumes are not mutually exclusive. This is the reason why these spectra are not additive.

We can isolate the low frequency features of this particular inter-band contribution from the conductivity measured experimentally by fitting the peak at 200 cm^{-1} to a Lorentz oscillator and subtracting it from the previously calculated inter-band conductivity. The resultant shows a roughly linear regime between 300 cm^{-1} and 950 cm^{-1} that can be fitted to a straight line with zero intercept (see figure 7(b)). With the assumption that this linearity is due to the Dirac dispersion, we can calculate the Fermi velocity using equation (1). There are four Dirac points in each Brillouin zone of YbMnBi_2 ¹⁶ and thus the calculated Fermi velocity is $(1.1 \pm 0.4) \times 10^5 \text{ cm/s}$ [or $0.045 \pm 0.01 \text{ eV} \cdot \text{\AA}$]. This estimated Fermi velocity is within the range expected from ARPES which varies between $9 \text{ eV} \cdot \text{\AA}$ (perpendicular to the k_x, k_y plane) and $0.043 \text{ eV} \cdot \text{\AA}$ (along k_z). As discussed before, anisotropic Dirac cones are a hallmark of AMnBi₂ compounds and our observations here on YbMnBi_2 fits well into this description. The existence of a Dirac fermionic dispersion is also in good agreement with the reported magnetotransport experiments²³.

We note that our interpretation of these peaks is at

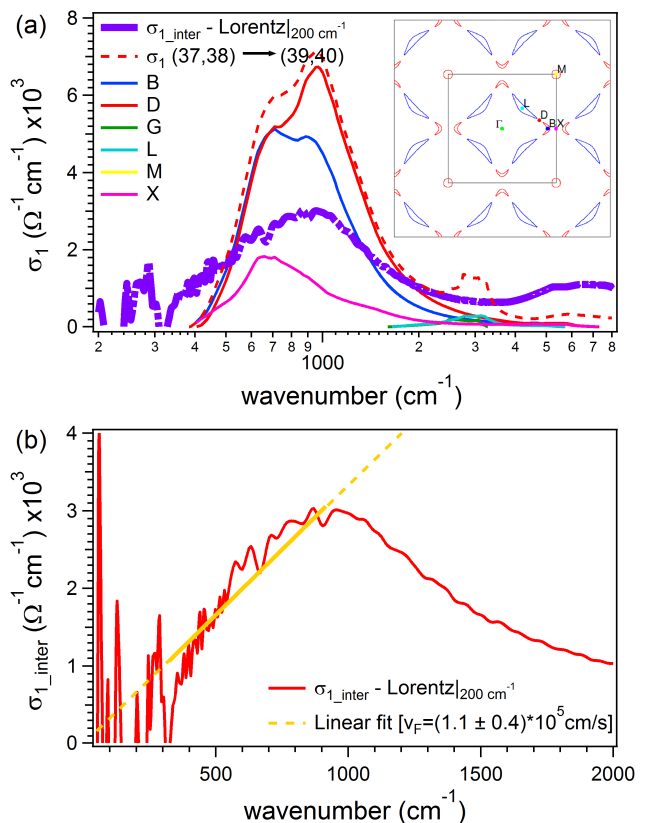


Figure 7. (a) Decomposition of the the inter-band contribution to the optical conductivity from the transition between the bands (37,38) \rightarrow (39,40) from different parts of the Fermi surface (fig. inset) (b) Linear fit of the inter-band transition peaked at 950 cm^{-1} .

odds with another recent optical study²⁵ that has observed similar features in low energy conductivity but proposes that the peak around 200 cm^{-1} derives from the van Hove singularity in a simplified WSM band structure. We do not favor this interpretation as realistic band structure calculations of YbMnBi_2 show it to exhibit certain non-idealities that will obscure the canonical behavior given in Ref.²³. Moreover, the Weyl state appears to be dependent on the existence of the magnetic structure for which there is no evidence. To reiterate, the the gross features of the optical response can be explained by the electronic structure of a uncanted state with a slightly shifted chemical potential.

IV. CONCLUSION

We have measured the reflectivity of YbMnBi_2 in the infrared regime and calculated the optical conductivity. The various features in the conductivity has been interpreted using DFT band structure calculations. We believe that the low energy peaks in conductivity at 200 cm^{-1} and 950 cm^{-1} are true inter-band transitions and the spectrum can be explained reasonably well without

invoking a canted magnetic structure which is necessary to realize Weyl nodes in this system. The conductivity leading up to the peak at 950 cm^{-1} is consistent with a linear Dirac dispersion with a small gap. Although canting of the Mn moments does improve the agreement of the calculated spectra with the experiments, similar effect can also be achieved by small shift in Fermi level. Precise control of the Fermi level in semimetals is rather difficult which when considering the lack evidence for canting, we believe makes the latter outcome more likely. However, in either case the high relative amplitude of the low energy peak is not apparent from band structure calculations but could be an manifestation of electronic correlation effects.

One must still reconcile the ARPES data that shows reasonably convincing evidence for Weyl physics¹⁶, with neutron scattering experiments^{19,20} that does not show evidence for canting and our optical data that does not need it. Moreover, we should reiterate that the crystal structure of this compound does not allow for a canted magnetic structure to develop through a second order phase transition. All of these considerations can be ac-

commodated if we assume that the reduced symmetry of the surface allows a surface magnetic structure reconstruction that is consistent with the canted state and a surface Weyl phase. It is possible that the surface of this compound hosts a true WSM through the breaking of time-reversal symmetry. Detailed measurements of the surface electronic structure or magnetism would be very useful in this regard.

V. ACKNOWLEDGEMENTS

We would like to thank C. Broholm, S. Borisenko and W. Fuhrman for helpful discussions and E. S. Arinze and N. Drichko for assistance with visible range reflectivity measurements. Optical measurements at JHU were supported by the U.S. Department of Energy, Office of Basic Energy Sciences under Contract DE-FG02-08ER46544. Sample growth at Princeton was supported by the ARO MURI on topological insulators, Grant W911NF-12-0461.

-
- ¹ J. Moore, *Nature Physics* **5**, 378 (2009).
- ² A. A. Burkov and L. Balents, *Phys. Rev. Lett.* **107**, 127205 (2011).
- ³ A. M. Turner, A. Vishwanath, and C. O. Head, *Topological Insulators* **6**, 293 (2013).
- ⁴ NP Armitage, EJ Mele, and Ashvin Vishwanath. Weyl and dirac semimetals in three dimensional solids. *arXiv preprint arXiv:1705.01111*, 2017.
- ⁵ X. Wan, A. Vishwanath, and S. Y. Savrasov, *Physical review letters* **108**, 146601 (2012).
- ⁶ X.-L. Qi and S.-C. Zhang, *Reviews of Modern Physics* **83**, 1057 (2011).
- ⁷ W. Witczak-Krempa, G. Chen, Y. B. Kim, and L. Balents, *Annual Review of Condensed Matter Physics* **5**, 57 (2014).
- ⁸ R. Schaffer, E. K.-H. Lee, B.-J. Yang, and Y. B. Kim, *arXiv preprint arXiv:1512.02224* (2015).
- ⁹ J. G. Rau, E. K.-H. Lee, and H.-Y. Kee, *arXiv preprint arXiv:1507.06323* (2015).
- ¹⁰ Y. F. Guo, A. J. Princep, X. Zhang, P. Manuel, D. Khalyavin, I. I. Mazin, Y. G. Shi, and A. T. Boothroyd, *Physical Review B* **90**, 075120 (2014).
- ¹¹ G. Lee, M. A. Farhan, J. S. Kim, and J. H. Shim, *Physical Review B* **87**, 245104 (2013).
- ¹² J. Park, G. Lee, F. Wolff-Fabris, Y. Koh, M. Eom, Y. Kim, M. Farhan, Y. Jo, C. Kim, J. H. Shim, and J. S. Kim, *Physical Review Letters* **107**, 126402 (2011).
- ¹³ K. Wang, D. Graf, L. Wang, H. Lei, S. Tozer, and C. Petrovic, *Physical Review B* **85**, 041101 (2012).
- ¹⁴ Y. Feng, Z. Wang, C. Chen, Y. Shi, Z. Xie, H. Yi, A. Liang, S. He, J. He, Y. Peng, *et al.*, *arXiv preprint arXiv:1312.0227* (2013).
- ¹⁵ A. F. May, M. A. McGuire, and B. C. Sales, *Phys. Rev. B* **90**, 075109 (2014).
- ¹⁶ S. Borisenko, D. Evtushinsky, Q. Gibson, A. Yaresko, T. Kim, M. Ali, B. Buechner, M. Hoesch, and R. J. Cava, *arXiv preprint arXiv:1507.04847* (2015).
- ¹⁷ A. B. Sushkov, J. B. Hofmann, G. S. Jenkins, J. Ishikawa, S. Nakatsuji, S. DasSarma, and H. D. Drew, *Physical Review B* **92**, 241108 (2015).
- ¹⁸ M. Hirschberger, S. Kushwaha, Z. Wang, Q. Gibson, C. A. Belvin, B. Bernevig, R. Cava, and N. Ong, *arXiv preprint arXiv:1602.07219* (2016).
- ¹⁹ W. Fuhrman, Q. Gibson, R. Cava, J. A. Rodriguez-Rivera, Y. Qiu, A. I. Kolesnikov, M. B. Stone, and C. Broholm, article in preparation.
- ²⁰ A. Wang, I. Zaliznyak, W. Ren, L. Wu, D. Graf, V. O. Garlea, J. B. Warren, E. Bozin, Y. Zhu, and C. Petrovic, *arXiv preprint arXiv:1604.01009* (2016).
- ²¹ P. Hosur and X. Qi, *Comptes Rendus Physique* **14**, 857 (2013).
- ²² B. Xu, Y. Dai, L. Zhao, K. Wang, R. Yang, W. Zhang, J. Liu, H. Xiao, G. Chen, A. Taylor, D. A. Yarotski, R. P. Prasankumar, X. G. Qiu, , *Physical Review B* **93**, 121110 (2016).
- ²³ C. J. Tabert and J. P. Carbotte, *Phys. Rev. B* **93**, 085442 (2016).
- ²⁴ D. Chaudhuri, B. Cheng, Q. D. Gibson, R. J. Cava, and N. P. Armitage, in *APS Meeting Abstracts* (2016).
- ²⁵ M. Chinotti, A. Pal, W. J. Ren, C. Petrovic, and L. Degiorgi, *Phys. Rev. B* **94**, 245101 (2016).
- ²⁶ O. K. Andersen, *Phys. Rev. B* **12**, 3060 (1975).
- ²⁷ V. Antonov, B. Harmon, and A. Yaresko, *Electronic structure and magneto-optical properties of solids* (Kluwer Academic Publishers, Dordrecht, Boston, London, 2004).
- ²⁸ J. P. Perdew and Y. Wang, *Phys. Rev. B* **45**, 13244 (1992).
- ²⁹ J. Perdew, K. Burke, and M. Ernzerhof, *Phys. Rev. Lett.* **77**, 3865 (1996).
- ³⁰ P. E. Blöchl, O. Jepsen, and O. K. Andersen, *Phys. Rev. B* **49**, 16223 (1994).

³¹ A. Kuzmenko, Review of Scientific Instruments **76**, 083108 (2005).

³² J. Allen and J. Mikkelsen, Physical Review B **15**, 2952 (1977).

³³ Supplementary Material.